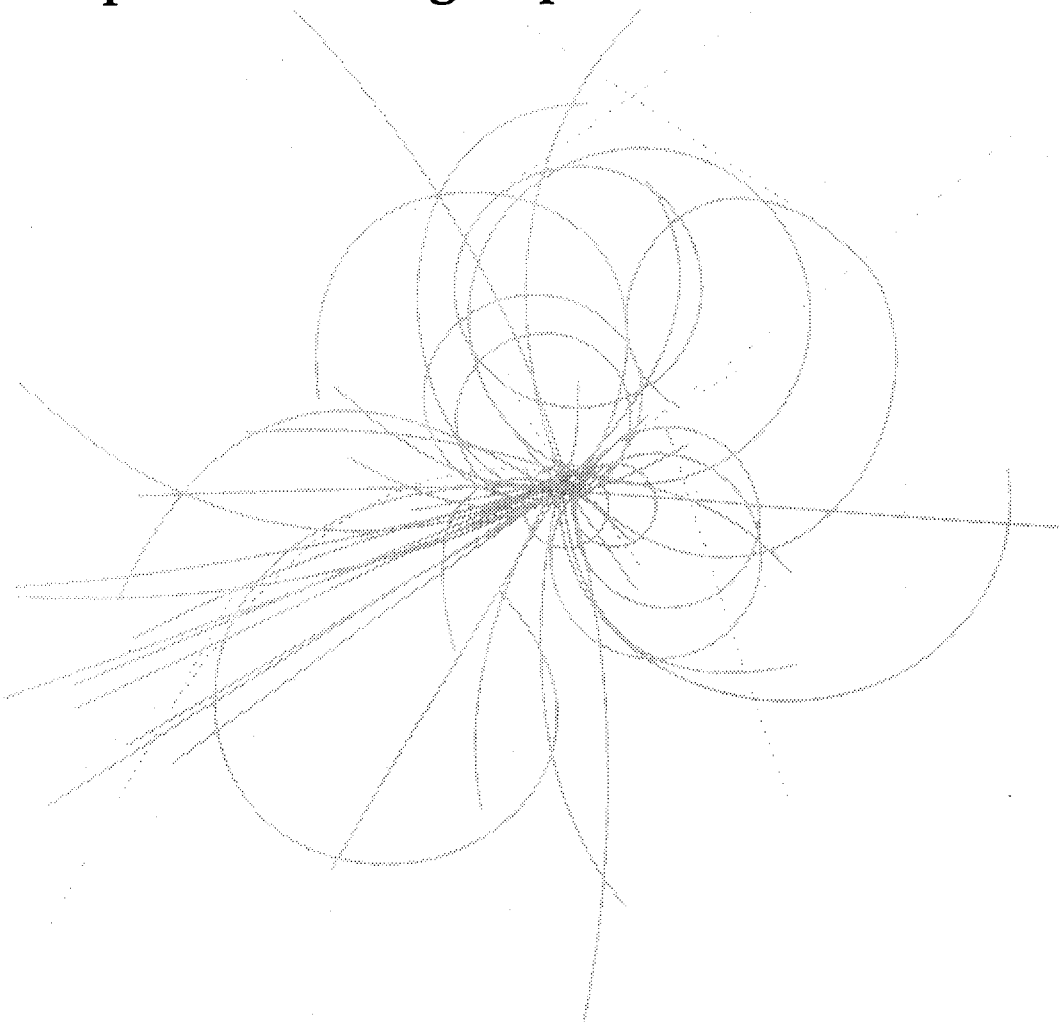


Superconducting Super Collider Laboratory



Reliability of Numerical Solutions of a Diffusion Equation Modeling RF Noise-Induced Dilution in Particle Beams

H.-J. Shih, J. Ellison, and W. Schiesser

July 1992

**Reliability of Numerical Solutions of a Diffusion Equation
Modeling RF Noise-Induced Dilution in Particle Beams***

H.-J. Shih, J. Ellison, and W. W. Schiesser

Superconducting Super Collider Laboratory[†]
2550 Beckleymeade Ave.
Dallas, TX 75237

July 1992

*Department of Mathematics and Statistics, University of New Mexico, Albuquerque, NM 87131.

[†]Operated by the Universities Research Association, Inc., for the U.S. Department of Energy under Contract No. DE-AC35-89ER40486.

RELIABILITY OF NUMERICAL SOLUTIONS OF A DIFFUSION EQUATION MODELING RF NOISE-INDUCED DILUTION IN PARTICLE BEAMS

H.-J. Shih, J. A. Ellison,* and W. E. Schiesser
Superconducting Super Collider Laboratory†
2550 Beckleymeade Avenue
Dallas, TX 75237

The dilution process in particle beams caused by noise in the rf accelerating system has been modeled using a diffusion equation. Particle tracking can also be undertaken to determine the effects of rf noise, though it is much more computationally extensive than integrating the diffusion equation. In this paper we present the integration results using the Method of Lines (MOL) for certain important classes of noise. We will describe the numerical algorithms in detail, including those that are made to remove anomalous solutions. Reliability of the numerical results will be checked using both finite-difference and finite-element (Galerkin) methods in discretization and applying the same algorithms to the cases of linear and quadratic diffusion coefficients where exact solutions are known.

1.0 THE DIFFUSION EQUATION

We begin this section with a brief description of motion of particles in a circular accelerator in order to indicate how the diffusion equation of interest arises. In a circular accelerator charged particles, guided by bending and focusing magnets, move along the design orbit in a horizontal plane. The deviations of motion from the design orbit in both horizontal and vertical directions constitute the transverse motion. A device, called the rf cavity, accelerates or decelerates the particles each time they pass through it by providing an electric voltage that varies in time sinusoidally. A synchronous particle, which moves on the design orbit at a constant momentum, will pass through the cavity at the zero crossing of the rf wave. The deviations in both momentum and phase from the synchronous particle constitute the longitudinal motion. The rf cavity is not noise-free; it has phase noise, which changes the synchronous phase, and amplitude noise, which changes the peak rf voltage. With rf noise, the longitudinal motion of a single particle is described by [1]

$$\dot{\phi} = P + \dot{\psi}(t), \quad (1.1a)$$

$$\dot{P} = -\Omega^2(1 + a(t)) \sin \phi, \quad (1.1b)$$

where P is a quantity proportional to the relative momentum deviation, ϕ the phase deviation, $\psi(t)$ the phase noise, and $a(t)$ the amplitude noise. Without rf noise, particles move on the closed orbits in the $P - \phi$ phase space, as shown in Figure 1. Under the perturbation of rf noise, particles gradually move onto bigger closed orbits and eventually cross over the so-called separatrix. When particles come close to the separatrix,

* Department of Mathematics and Statistics, University of New Mexico, Albuquerque, NM 87131.

† Operated by the Universities Research Association, Inc., for the U.S. Department of Energy under Contract No. DE-AC35-89ER40486.

a device called the collimator is usually employed to remove them from the beam. This defines a critical orbit beyond which particles are removed.

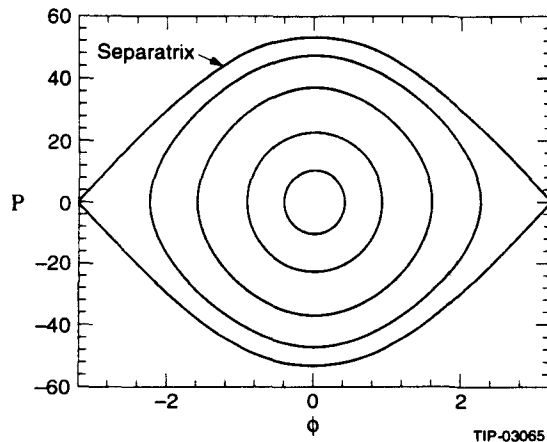


Figure 1. Particle orbits in longitudinal phase space.

If we define action (times 2π) to be the area in the $P - \phi$ phase space enclosed by the unperturbed closed orbit, then the effect of rf noise is to induce a diffusion of particles in action. There is now a good theoretical model [1] in which this diffusion process is approximated by a Markov process, and the evolution of the probability density in action, $\rho(x, t)$, is governed by the following diffusion equation:

$$\frac{\partial \rho}{\partial t} = \frac{\partial}{\partial x} \left(D(x) \frac{\partial \rho}{\partial x} \right). \quad (1.2)$$

Here x is the normalized action with $x = 1$ at the critical orbit, and $D(x)$ is the diffusion coefficient. The theory gives provision for computing the diffusion coefficient from the noise spectral density. In Figure 2 we show the diffusion coefficients for four types of noise: white phase, notched phase, white amplitude, and notched amplitude. In the white noise cases, the spectral density is constant in the entire range of frequency. The notched noise cases are obtained from the white noise cases by filtering out a range of frequency components of the noise. This results in a discontinuous diffusion coefficient for notched noise, as can be seen in Figure 2. It can be shown from the theory (and indeed is seen in Figure 2) that the asymptotic behaviors of the diffusion coefficients for small x are: $D(x) \sim x$ for white phase noise, $D(x) \sim x^2$ for white amplitude noise, $D(x) \sim x^3$ for notched phase noise, and $D(x) \sim x^4$ for notched amplitude noise. If we identify $D(\partial\rho/\partial x)$ as the probability flux, Eq. (1.2) just expresses conservation of probability. It is obvious that there cannot be any flux crossing $x = 0$, so the boundary condition at $x = 0$ is

$$D(0) \frac{\partial \rho}{\partial x}(0, t) = 0. \quad (1.3)$$

For our application this condition is always satisfied because $D(0) = 0$ and $\partial\rho/\partial x$ is bounded. Since particles are removed at the critical orbit, the boundary condition at $x = 1$ is

$$\rho(1, t) = 0. \quad (1.4)$$

The definition of $\rho(x, t)$ is completed by specifying the initial condition

$$\rho(x, 0) = \rho_0(x), \quad (1.5)$$

where $\rho_0(x)$ is determined from the distributions of particles in P and ϕ which, to a good approximation, we take to be Gaussian.

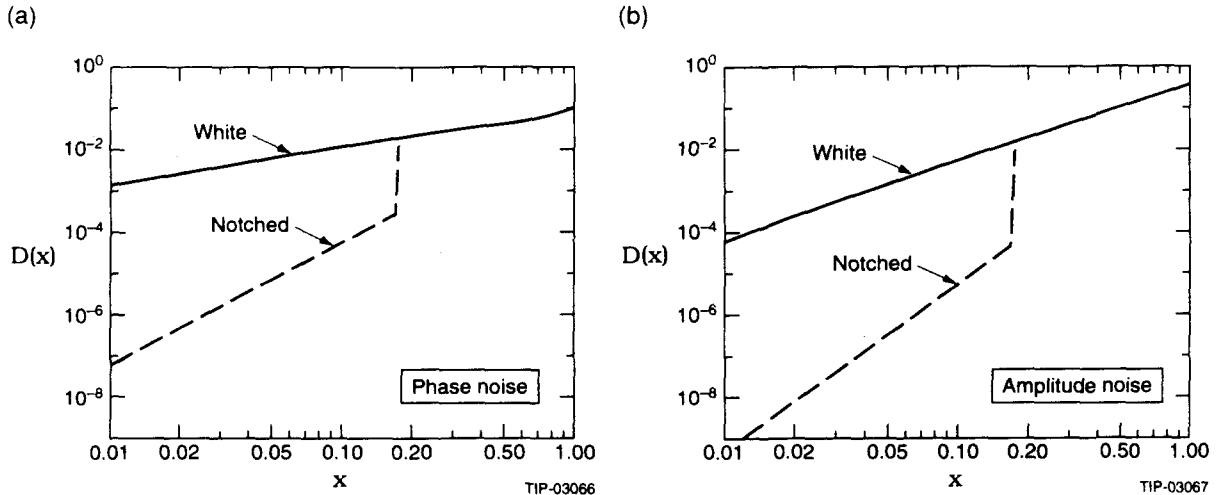


Figure 2. Diffusion coefficients for noise in the rf cavity. (a) Phase noise. (b) Amplitude noise. Solid line: white case; dashed line: notched case.

We have used the numerical Method of Lines (MOL) [2] to integrate the diffusion equation with the diffusion coefficients given in Figure 2. The system of ODEs in time resulting from discretizing the partial derivatives with respect to x is integrated by the nonstiff solver RKF45 [3] or the stiff solver LSODES [4]. It appears that our system of ODEs is stiff, for we have found that the computing time using LSODES is less by a factor of 5 to 10 than it is using RKF45. Because we obtain essentially identical numerical solutions using these two solvers, we will present only the results from LSODES.

Since we don't have exact solutions for the diffusion coefficients shown in Figure 2, and since we observe numerical anomalies in some cases, it is then necessary to check the reliability of our numerical solutions. We have done this in three ways: (1) We employ two different methods (finite-difference and Galerkin finite-element) to discretize the partial derivatives with respect to x . (2) We check if our solutions don't change with an increasingly larger number of grid points or basis functions in the two discretization methods. (3) We apply the same numerical procedure to the cases of $D(x) = x$ and x^2 for which we know the exact solutions.

This paper is organized as follows: (1) In Section 2.0 we describe our discretization algorithms, including those that we use to remove the numerical anomalies. (2) In Section 3.0 we integrate the diffusion equation for the diffusion coefficients shown in Figure 2 and discuss the reliability of our numerical results. (3) In Section 4.0 we integrate the diffusion equation for $D(x) = x$ and x^2 and compare with the exact solutions. (4) Conclusions are given in Section 5.0.

2.0 MOL DISCRETIZATION

2.1 Finite-difference Methods

In our standard finite-difference method, a uniform grid, with the grid points at $x_1 = 0, x_2 = \Delta x, x_3 = 2\Delta x, \dots, x_N = (N-1)\Delta x = 1$, is used, and the following three-point, second-order formulas [2] are then employed to approximate the partial derivatives of function $f(x, t)$ with respect to x at grid point i :

$$\begin{aligned}
 f_{x,i \neq 1,N} &= \frac{1}{2\Delta x}(f_{i+1} - f_{i-1}) \\
 f_{x,i=1} &= \frac{1}{2\Delta x}(-3f_1 + 4f_2 - f_3) \\
 f_{x,i=N} &= \frac{1}{2\Delta x}(f_{N-2} - 4f_{N-1} + 3f_N).
 \end{aligned}
 \tag{2.1}$$

Here f_x denotes the partial derivative of f with respect to x , and the subscript i denotes the value of f or f_x at grid point i . Discretization of the left-hand side of Eq. (1.2) at grid point i proceeds in three steps: (1) Eq. (2.1) is used to obtain $\rho_{x,i}$. (2) $D(x_i)$ is multiplied by $\rho_{x,i}$. (3) Eq. (2.1) is used again to obtain $(D\rho_x)_{x,i}$. To ensure the absorbing boundary condition at $x = 1$ (grid point $i = N$), we always set $\rho_{t,i=N} = 0$.

However, the standard method gives anomalous results in some cases, as we will see in Section 3.0, so we have two variations of it that we describe below. Variation I is used to deal with the case where the density at the origin is fixed and the slope there steepens in time. This can occur when $D(x) \sim x^2$ as x approaches 0, since $\rho_t = D_x \rho_x + D \rho_{xx}$ (from Eq. (1.2)) and $(\rho_x)_t = D_{xx} \rho_x + 2D_x \rho_{xx} + D \rho_{xxx}$, and thus $\rho_t = 0$ and $(\rho_x)_t \sim \rho_x$ at $x = 0$. To obtain a better approximation of partial derivatives with respect to x near $x = 0$, we use a variable grid with a finer mesh near $x = 0$. Specifically, the grid points are generated by

$$x_i = \frac{i(i-1)d}{2}, \quad i = 1, 2, \dots, N, \quad (2.2)$$

where d is the spacing between the first and second grid points. Since $x_N = 1$, we have

$$d = \frac{2}{N(N-1)}. \quad (2.3)$$

A feature of this variable grid is that the spacing between two successive grid points is linearly increasing with i . The approximation of the left-hand side of Eq. (1.2) is given by

$$\begin{aligned} \rho_{t,i \neq 1,N} &\cong \frac{2}{\Delta x_i + \Delta x_{i-1}} \left(\frac{D_{i+1} + D_i}{2} \frac{\rho_{i+1} - \rho_i}{\Delta x_i} - \frac{D_i + D_{i-1}}{2} \frac{\rho_i - \rho_{i-1}}{\Delta x_{i-1}} \right), \\ \rho_{t,i=1} &\cong \frac{2}{\Delta x_1} \left(\frac{D_2 + D_1}{2} \frac{\rho_2 - \rho_1}{\Delta x_1} - 0 \right), \\ \rho_{t,i=N} &= 0. \end{aligned} \quad (2.4)$$

Here $\Delta x_i = x_{i+1} - x_i$, and we have approximated the flux at the center between grid points i and $i+1$ by

$$(D\rho_x)_i \approx \frac{D_{i+1} + D_i}{2} \frac{\rho_{i+1} - \rho_i}{\Delta x_i}. \quad (2.5)$$

Also we have used the fact that the flux at $x = 0$ (grid point $i = 1$) is zero.

Variation II is used to deal with the case where the diffusion coefficient is discontinuous at some x . The integration of the diffusion equation is done not only at the grid points in a uniform grid but also at the discontinuity point to preserve conservation of probability across that point. The following approximations are employed at the discontinuity point x_c and its two neighboring grid points x_j and x_{j+1} ($x_j < x_c < x_{j+1}$):

$$\begin{aligned} \rho_{t,j} &\approx \frac{2}{\Delta x^- + \Delta x} \left(\frac{D_c^- + D_j}{2} \frac{\rho_c - \rho_j}{\Delta x^-} - \frac{D_j + D_{j-1}}{2} \frac{\rho_j - \rho_{j-1}}{\Delta x} \right), \\ \rho_{t,c} &\approx \frac{2}{\Delta x^- + \Delta x^+} \left(\frac{D_{j+1} + D_c^+}{2} \frac{\rho_{j+1} - \rho_c}{\Delta x^+} - \frac{D_c^- + D_j}{2} \frac{\rho_c - \rho_j}{\Delta x^-} \right), \\ \rho_{t,j+1} &\approx \frac{2}{\Delta x + \Delta x^+} \left(\frac{D_{j+2} + D_{j+1}}{2} \frac{\rho_{j+2} - \rho_{j+1}}{\Delta x} - \frac{D_{j+1} + D_c^+}{2} \frac{\rho_{j+1} - \rho_c}{\Delta x^+} \right). \end{aligned} \quad (2.6)$$

where ρ_c is the action density at x_c ; D_c^+ and D_c^- are the limiting values of the diffusion coefficient at x_c from the right and left sides, respectively; $\Delta x^- = x_c - x_j$; and $\Delta x^+ = x_{j+1} - x_c$. For other grid points, the approximations (2.4) are used.

2.2 Galerkin Method

In our Galerkin approximation [5] of $\rho(x, t)$

$$\rho_G(x, t) = \sum_{i=1}^N C_i(t) \Phi_i(x). \quad (2.7)$$

the basis functions $\Phi_i(x)$ are piecewise linear, as shown in Figure 3(a). Here $\Phi_i(x)$ is centered at x_i , and the centers are equally spaced by $\Delta x = 1/(N - 1)$. The derivatives of $\Phi_i(x)$, $\Phi'_i(x)$, are shown in Figure 3(b).

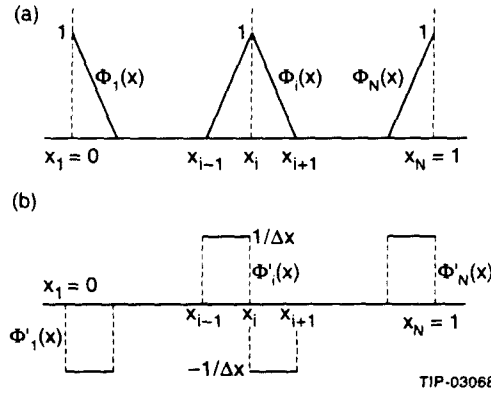


Figure 3. (a) Basis functions in the Galerkin approximation. (b) Derivatives of (a).

The system of ODEs for time-dependent coefficients $C_i(t)$ are determined by applying the Galerkin condition

$$\int_0^1 \Phi_j(x) R(x, t) dx = 0 \quad (2.8)$$

for each basis function. Here the residual function $R(x, t)$ is defined by

$$R(x, t) = \frac{\partial \rho_G}{\partial t} - \frac{\partial}{\partial x} \left(D(x) \frac{\partial \rho_G}{\partial x} \right). \quad (2.9)$$

The absorbing boundary condition at $x = 1$ gives

$$C_N(t) = \sum_{i=1}^N C_i(t) \Phi_i(x_N) = \rho(x_N, t) = 0,$$

which follows from $\Phi_N(x_N) = 1$ and $\Phi_i(x_N) = 0$ for $i \neq N$ in Figure 3(a). Thus we need only determine $C_i(t)$, $i = 1, 2, \dots, N - 1$. Let

$$\mathbf{C}(t) = \begin{pmatrix} C_1(t) \\ C_2(t) \\ \vdots \\ C_{N-1}(t) \end{pmatrix}. \quad (2.10a)$$

Then the system of ODEs for $C_i(t)$ is given by

$$\mathbf{C}'(t) = (\mathbf{A}^{-1}\mathbf{B})\mathbf{C}(t). \quad (2.10b)$$

$$\mathbf{A} = \frac{\Delta x}{6} \begin{pmatrix} 2 & 1 & 0 & 0 & \dots & 0 \\ 1 & 4 & 1 & 0 & \dots & 0 \\ 0 & 1 & 4 & 1 & \dots & 0 \\ \vdots & & & & & \vdots \\ 0 & \dots & 0 & 1 & 4 & 1 \\ 0 & \dots & 0 & 0 & 1 & 4 \end{pmatrix} \quad (2.10c)$$

$$\mathbf{B} = \frac{1}{\Delta x^2} \begin{pmatrix} -d_1 & d_1 & 0 & 0 & \dots & 0 \\ d_1 & -(d_1 + d_2) & d_2 & 0 & \dots & 0 \\ 0 & d_2 & -(d_2 + d_3) & d_3 & \dots & 0 \\ \vdots & & & & & \vdots \\ 0 & \dots & 0 & d_{N-3} & -(d_{N-3} + d_{N-2}) & d_{N-2} \\ 0 & \dots & 0 & 0 & d_{N-2} & -(d_{N-2} + d_{N-1}) \end{pmatrix} \quad (2.10d)$$

Here d_i is the integral of $D(x)$ from x_i to x_{i+1} . To obtain Eq. (2.10), we note that for $j = 1, 2, \dots, N-1$, we have

$$\int_0^1 \Phi_j(x) \frac{\partial}{\partial t} \rho_G(x, t) dx = \int_0^1 \Phi_j(x) \left(\sum_{i=1}^{N-1} C_i'(t) \Phi_i(x) \right) dx, \quad (2.11a)$$

and

$$\begin{aligned} & \int_0^1 \Phi_j(x) \frac{\partial}{\partial x} \left(D(x) \frac{\partial}{\partial x} \rho_G(x, t) \right) dx \\ &= \left(\Phi_j(x) D(x) \frac{\partial}{\partial x} \rho_G(x, t) \right)_{x=0}^{x=1} - \int_0^1 \left(D(x) \frac{\partial}{\partial x} \rho_G(x, t) \right) \Phi_j'(x) dx \\ &= - \int_0^1 \left(D(x) \frac{\partial}{\partial x} \rho_G(x, t) \right) \Phi_j'(x) dx \\ &= - \int_0^1 D(x) \left(\sum_{i=1}^{N-1} C_i(t) \Phi_i'(x) \right) \Phi_j'(x) dx. \end{aligned} \quad (2.11b)$$

For $j = 1$, Eq. (2.11a) becomes

$$\begin{aligned}
& \sum_{i=1}^{N-1} C'_i(t) \int_0^1 \Phi_1(x) \Phi_i(x) dx \\
&= C'_1(t) \int_0^1 \Phi_1(x) \Phi_1(x) dx + C'_2(t) \int_0^1 \Phi_1(x) \Phi_2(x) dx \\
&= C'_1(t) \left(\frac{\Delta x}{3} \right) + C'_2(t) \left(\frac{\Delta x}{6} \right) \\
&= \frac{\Delta x}{6} (2C'_1(t) + C'_2(t)).
\end{aligned} \tag{2.12a}$$

which follows from the properties of $\Phi_i(x)$ shown in Figure 3(a), and Eq. (2.11b) becomes

$$\begin{aligned}
& - \sum_{i=1}^{N-1} C_i(t) \int_0^1 D(x) \Phi'_i(x) \Phi'_1(x) dx \\
&= -C_1(t) \int_0^1 D(x) \Phi'_1(x) \Phi'_1(x) dx - C_2(t) \int_0^1 D(x) \Phi'_2(x) \Phi'_1(x) dx \\
&= -C_1(t) \int_{x_1}^{x_2} D(x) \left(-\frac{1}{\Delta x} \right) \left(-\frac{1}{\Delta x} \right) dx - C_2(t) \int_{x_1}^{x_2} D(x) \left(+\frac{1}{\Delta x} \right) \left(-\frac{1}{\Delta x} \right) dx \\
&= \frac{1}{\Delta x^2} (-C_1(t)d_1 + C_2(t)d_1),
\end{aligned} \tag{2.12b}$$

which follows from the properties of $\Phi'_i(x)$ shown in Figure 3(b). For $j = 2, 3, \dots, N-1$, Eq. (2.11a) becomes

$$\begin{aligned}
& \sum_{i=1}^{N-1} C'_i(t) \int_0^1 \Phi_j(x) \Phi_i(x) dx \\
&= C'_{j-1}(t) \int_0^1 \Phi_j(x) \Phi_{j-1}(x) dx + C'_j(t) \int_0^1 \Phi_j(x) \Phi_j(x) dx \\
&\quad + C'_{j+1}(t) \int_0^1 \Phi_j(x) \Phi_{j+1}(x) dx \\
&= C'_{j-1}(t) \left(\frac{\Delta x}{6} \right) + C'_j(t) \left(\frac{2\Delta x}{3} \right) + C'_{j+1}(t) \left(\frac{\Delta x}{6} \right) \\
&= \frac{\Delta x}{6} (C'_{j-1}(t) + 4C'_j(t) + C'_{j+1}(t)).
\end{aligned} \tag{2.13a}$$

and Eq. (2.11b) becomes

$$\begin{aligned}
& - \sum_{i=1}^{N-1} C_i(t) \int_0^1 D(x) \Phi'_i(x) \Phi'_j(x) dx \\
& = -C_{j-1}(t) \int_0^1 D(x) \Phi'_{j-1}(x) \Phi'_j(x) dx - C_j(t) \int_0^1 D(x) \Phi'_j(x) \Phi'_j(x) dx \\
& \quad - C_{j+1}(t) \int_0^1 D(x) \Phi'_{j+1}(x) \Phi'_j(x) dx \\
& = -C_{j-1}(t) \int_{x_{j-1}}^{x_j} D(x) \left(-\frac{1}{\Delta x} \right) \left(+\frac{1}{\Delta x} \right) dx - C_j(t) \int_{x_{j-1}}^{x_j} D(x) \left(+\frac{1}{\Delta x} \right) \left(+\frac{1}{\Delta x} \right) dx \\
& \quad - C_j(t) \int_{x_j}^{x_{j+1}} D(x) \left(-\frac{1}{\Delta x} \right) \left(-\frac{1}{\Delta x} \right) dx - C_{j+1}(t) \int_{x_j}^{x_{j+1}} D(x) \left(-\frac{1}{\Delta x} \right) \left(+\frac{1}{\Delta x} \right) dx \\
& = \frac{1}{\Delta x^2} (C_{j-1}(t)d_{j-1} - C_j(t)(d_{j-1} + d_j) + C_{j+1}(t)d_j).
\end{aligned} \tag{2.13b}$$

Again, Eq. (2.13) follows from the properties of $\Phi_i(x)$ shown in Figure 3. Equation (2.10) is then obtained by equating Eqs. (2.12a) and (2.12b) for $j = 1$, and Eqs. (2.13a) and (2.13b) for $j = 2, 3, \dots, N - 1$.

3.0 NUMERICAL RESULTS FOR RF NOISE

Figure 4 shows the integration results for white phase noise and $N = 251$ in time steps of 2. The dashed line is the initial distribution, the solid curves are results from the standard finite-difference method, and the crosses are from the Galerkin method. They are in very good agreement. We have also checked that the numerical results in each method are essentially the same for $N = 501$.

Figure 5 shows the integration results for white amplitude noise and $N = 251$ in time steps of 1 from the standard finite-difference method. Here we observe some numerical anomaly: oscillations appear and become more pronounced as time progresses. We have mentioned in Section 1.0 that the diffusion coefficient for white amplitude noise is quadratic near $x = 0$. Thus, according to the discussion in Section 2.1, $\rho(0, t)$ is fixed and $\rho_x(0, t)$ increases in magnitude in time, leading to poorer approximation in time for ρ_x near $x = 0$ in the finite-difference method with a uniform grid. This is probably the cause of the anomaly we observe in Figure 5. To resolve this, we employ finite-difference method variation I in which, as mentioned in Section 2.1, the grid is finer near $x = 0$. Figure 6 shows the integration results in time steps of 2 for $N = 251$ (solid curves) and for $N = 101$ (crosses). They are in very good agreement. This approach seems to give results that converge sooner. The integration results using the Galerkin method are shown, by crosses, in Figure 7(a) for $N = 251$, and in Figure 7(b) for $N = 501$. Also shown in these figures, by solid curves, are the results for $N = 251$ using finite-difference method variation I. Here we see that the Galerkin results converge more slowly than the results using finite-difference method variation I.

Figure 8 shows the integration results for notched phase noise and $N = 251$ from the standard finite-difference method. Here again we observe numerical anomaly: oscillations similar to those in Figure 5 occur, though they seem to diminish as time progresses. Since the diffusion coefficient is discontinuous in this case, and since the discontinuity point is not one of the grid points, we suspect the anomaly is caused by

the inaccurate approximation of the fluxes on either side of the discontinuity point. To settle this, we employ finite-difference method variation II in which, as mentioned in Section 2.1, an extra difference equation at the discontinuity point is also integrated. Figure 9 shows the results using this approach for $N = 251$ (solid curves) in time steps of 4, as well as the Galerkin results for $N = 251$ (crosses). Both are in very good agreement. Here the Galerkin method appears more robust. Since the results for notched amplitude noise are similar to those for notched phase noise, they are not presented here.

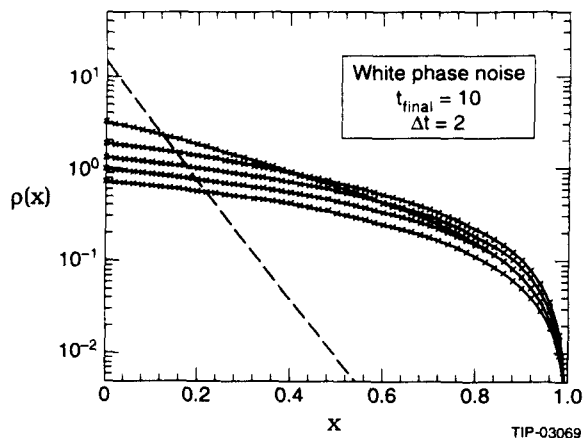


Figure 4. Integration results in time steps of 2 for white phase noise (whose diffusion coefficient is shown in Figure 2(a)) and $N = 251$. Solid curves: standard finite-difference; crosses: Galerkin. The dashed line is the initial distribution.

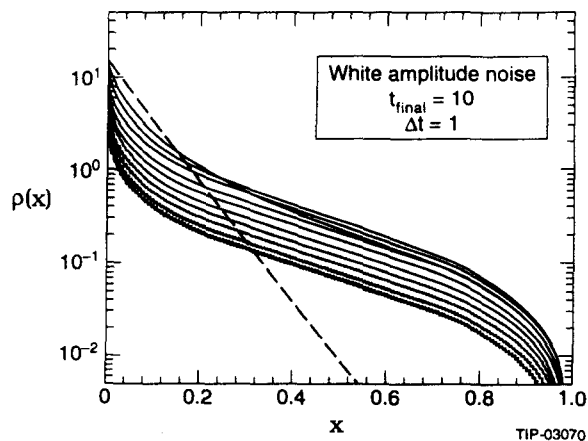


Figure 5. Integration results in time steps of 1 for white amplitude noise (whose diffusion coefficient is shown in Figure 2(b)). The standard finite-difference method with $N = 251$ is used in discretization. The dashed line is the initial distribution.

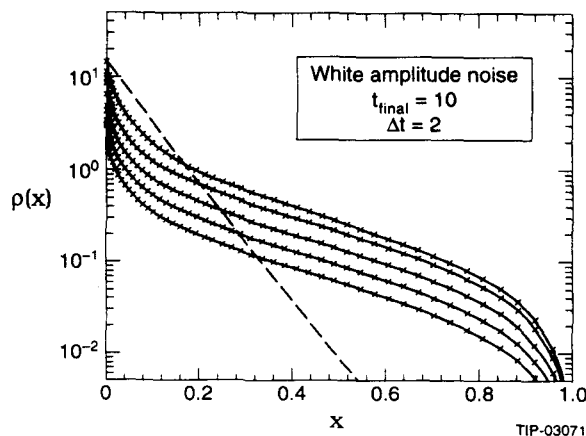


Figure 6. Integration results in time steps of 2 for same white amplitude noise as in Figure 5. Finite-difference variation I is used in discretization. Solid curves: $N = 251$; crosses: $N = 101$. The dashed line is the initial distribution.

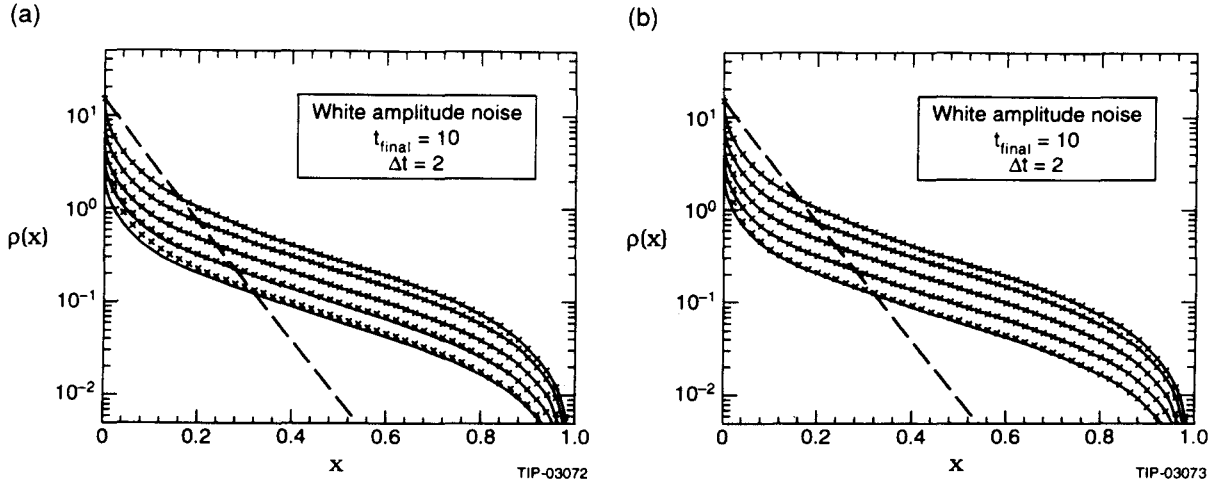


Figure 7. Same as Figure 6, except that crosses are the Galerkin results. (a) $N = 251$. (b) $N = 501$.

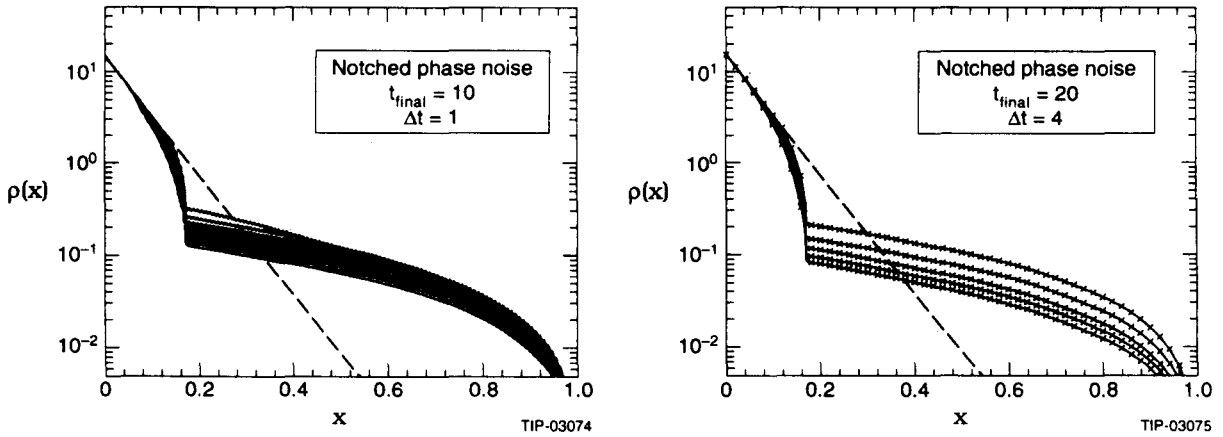


Figure 8. Integration results in time steps of 1 for notched phase noise (whose diffusion coefficient is shown in Figure 2(a)) and $N = 251$. The standard finite-difference method is used in discretization. The dashed line is the initial distribution.

Figure 9. Integration results in time steps of 4 for same notched phase noise as in Figure 8 and $N = 251$. Solid curves: finite-difference variation II; crosses: Galerkin. The dashed line is the initial distribution.

4.0 SOLUTIONS OF THE $D(x) = x$ AND x^2 CASES

4.1 Case of $D(x) = x$

The general solution in this case is found by separation of variables to be

$$\rho(x, t) = \sum_{n=1}^{\infty} a_n e^{-\lambda_n^2 t/4} J_0(\lambda_n \sqrt{x}). \quad (4.1)$$

where J_0 is the Bessel Function of order zero and λ_n is the n th root of J_0 . To test our numerical procedure, we have simply used the $n = 1$ term:

$$\rho_1(x, t) = a_1 e^{-\lambda_1^2 t/4} J_0(\lambda_1 \sqrt{x}). \quad (4.2a)$$

where a_1 is given by

$$a_1 = \frac{\lambda_1}{2J_1(\lambda_1)} \quad (4.2b)$$

so that the integral from 0 to 1 of $\rho(x, t)$ is normalized to 1 at $t = 0$.

Figure 10 compares the exact solutions with the integration results for $N = 251$ in time steps of 0.2. The dashed line is the initial distribution; the solid curves are the exact solutions; and crosses and circles represent the results from standard finite-difference and Galerkin, respectively. They are all in good agreement with the exact solutions.

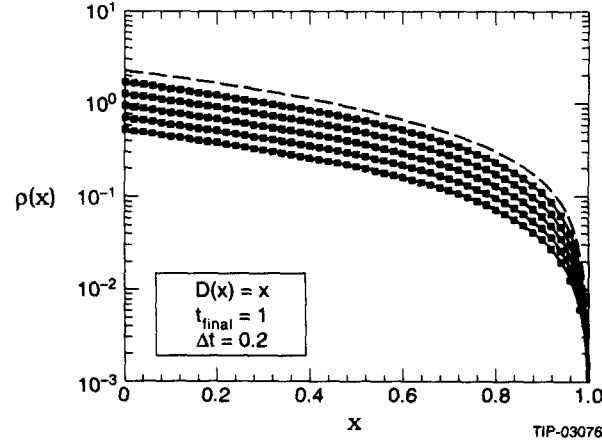


Figure 10. Integration results and exact solutions in time steps of 0.2 for $D(x) = x$. Solid curves: exact solutions; crosses: standard finite-difference with $N = 251$; circles: Galerkin with $N = 251$. The dashed line is the initial distribution.

4.2 Case of $D(x) = x^2$

The general solution in this case is given by

$$\rho(x, t) = \frac{2}{\pi} x^{-\frac{1}{2}} \int_0^{\infty} \left(\int_0^{\infty} e^{-\xi/2} \rho_0(e^{-\xi}) \sin(\mu\xi) d\xi \right) e^{-(\mu^2 + \frac{1}{4})t} \sin(-(\ln x)\mu) d\mu, \quad (4.3)$$

where $\rho_0(x) = \rho(x, 0)$. We outline the derivation of this solution below. Under the transformation

$$y = -\ln x \quad (4.4a)$$

$$\rho(x, t) = x^{-\frac{1}{2}} \psi(y, t) \quad (4.4b)$$

we obtain in place of Eqs. (1.2), (1.4), and (1.5) the following equivalent problem

$$\begin{aligned}
v_t &= v_{yy} - \frac{1}{4}v \\
v(0, t) &= 0 \\
v(y, 0) &= v_0(y) = \epsilon^{-y/2} \rho_0(\epsilon^{-y}).
\end{aligned} \tag{4.5}$$

For $\lambda < 1/4$, the function φ defined by $v(y, t) = \epsilon^{-\lambda t} \varphi(y, \lambda)$ cannot satisfy the boundary condition if φ is nontrivial and finite. For $\lambda \geq 1/4$, we have

$$\varphi(y, \lambda) \propto \sin\left(\sqrt{\lambda - \frac{1}{4}} y\right). \tag{4.6}$$

Therefore, one can seek a solution of the form

$$\psi(y, t) = \int_{\frac{1}{4}}^{\infty} A(\lambda) e^{-\lambda t} \sin\left(\sqrt{\lambda - \frac{1}{4}} y\right) d\lambda. \tag{4.7}$$

From the Fourier integral theorem, it is easy to show

$$A(\lambda) = \frac{1}{\pi \sqrt{\lambda - \frac{1}{4}}} \int_0^{\infty} \psi_0(\xi) \sin\left(\sqrt{\lambda - \frac{1}{4}} \xi\right) d\xi. \tag{4.8}$$

We now have a complete solution, namely Eqs. (4.4b), (4.7) and (4.8). Equation (4.3) is then obtained under the change of variable from λ to $\mu = \sqrt{\lambda - 1/4}$.

If the initial condition $u_0(x)$ is a polynomial, the two infinite integrals in Eq. (4.3) can be evaluated analytically. This involves two steps: (1) The inner integral is then a sum of terms of the form (Ref. 6, p. 477)

$$\int_0^{\infty} e^{-c\xi} \sin(\mu\xi) d\xi = \frac{\mu}{c^2 + \mu^2}. \tag{4.9}$$

(2) The outer integral is then a sum of terms of the form (Ref. 6, p. 497)

$$\begin{aligned}
& \int_0^{\infty} \frac{\mu}{c^2 + \mu^2} e^{-b\mu^2} \sin(a\mu) d\mu \\
&= -\frac{\pi}{4} \epsilon^{bc^2} \left[2 \sinh(ac) + \epsilon^{-ac} \Phi\left(\sqrt{bc} - \frac{a}{2\sqrt{b}}\right) - \epsilon^{ac} \Phi\left(\sqrt{bc} + \frac{a}{2\sqrt{b}}\right) \right] \\
&\equiv F(a, b, c).
\end{aligned} \tag{4.10}$$

where Φ is the error function defined by $\Phi(x) = (2/\sqrt{\pi}) \int_0^x e^{-t^2} dt$. In testing our numerical procedure, we have used $u_0(x) = 3(x-1)^2$. In this case, the exact solution is given by

$$\rho(x, t) = \frac{6}{\pi} x^{-\frac{1}{2}} \epsilon^{-\frac{1}{4}} \left\{ F\left(-\ln x, t, \frac{5}{2}\right) - 2F\left(-\ln x, t, \frac{3}{2}\right) + F\left(-\ln x, t, \frac{1}{2}\right) \right\}. \quad (4.11)$$

Figure 11 compares in time steps of 1 the exact solutions (solid curves) with the integration results (crosses) for $N = 101$ from finite-difference method variation I. The results from the Galerkin method (crosses) are compared to the exact solutions (solid curves) in Figure 12(a) for $N = 101$, and in Figure 12(b) for $N = 251$. As in the case of white amplitude noise whose diffusion coefficient is quadratic near $x = 0$, results from the Galerkin method converge more slowly toward the exact solutions.

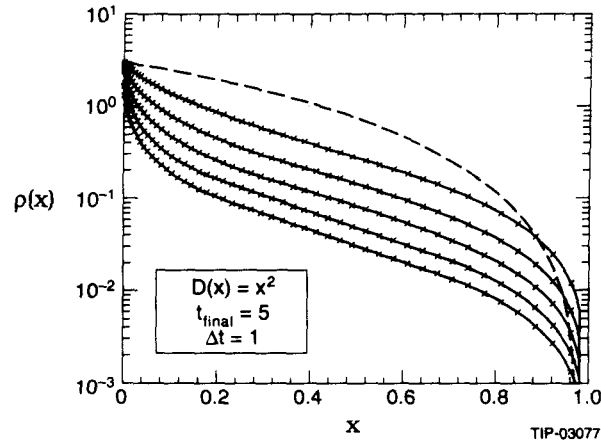


Figure 11. Integration results and exact solutions in time steps of 1 for $D(x) = x^2$. Solid curves: exact solutions; crosses: finite-difference variation I with $N = 101$. The dashed line is the initial distribution.

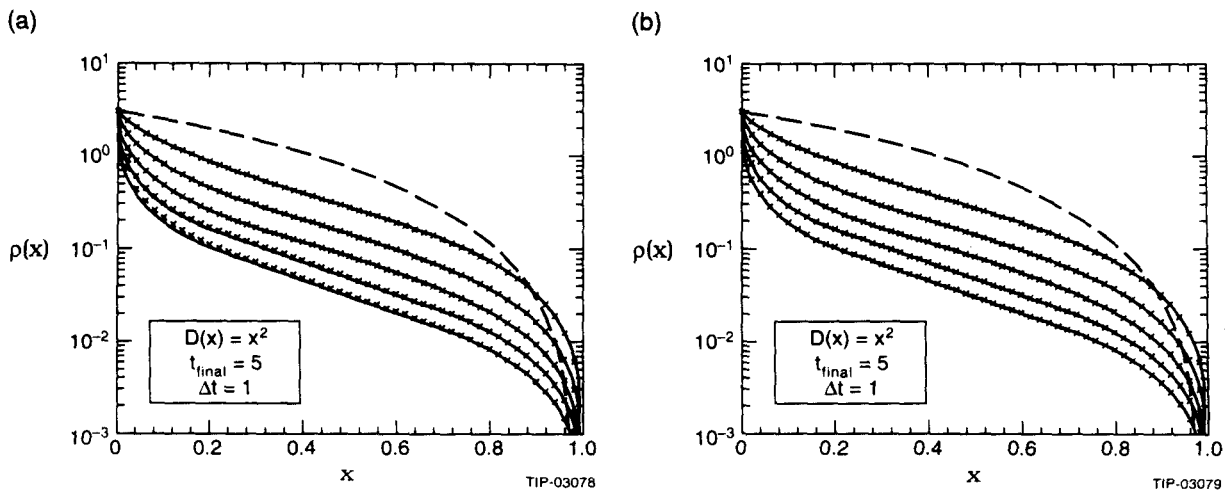


Figure 12. Same as Figure 11, except that crosses are the Galerkin results. (a) $N = 101$. (b) $N = 251$.

5.0 CONCLUDING REMARKS

A code has been developed to solve the diffusion equation (1.2) with the boundary conditions (1.3) and (1.4) using the numerical Method of Lines. Finite-difference or Galerkin finite-element approximations are used to convert the PDE to a system of ODEs, which are then integrated by the nonstiff solver RKF45 or the stiff solver LSODES. The code includes (1) computation of the diffusion coefficient from the spectral density for noise in the rf accelerating system, and (2) computation of the distribution of the beam in action from Gaussian or any other distributions in longitudinal phase space. From the discussions above, we believe the code gives reliable numerical results and is most efficient when finite-difference approximations (with suitable modifications) and the stiff solver LSODES are used. The modifications made to remove anomalous results from the finite-difference method with a uniform grid are also implemented in the code. Though very robust (in the sense that it always gives smooth solutions), the Galerkin method, as it is now implemented in the code, is not very computationally efficient. The efficiency presumably can be improved by taking advantage of the sparseness of the matrices involved and by using a non-uniform grid; however, our main interest here was in checking the finite-difference results. The code will be available upon request from the authors.

REFERENCES

- [1] G. Dôme, "Diffusion Due to RF Noise," in *CERN Advanced Accelerator School on Advanced Accelerator Physics*, CERN Report No. 87-03, 1987, pp. 370–401.
- [2] W.E. Schiesser, *The Numerical Method of Lines Integration of Partial Differential Equations*, Academic Press, San Diego, CA, 1991.
- [3] G.E. Forsythe, M.A. Malcolm, and C.B. Moler, *Computer Methods for Mathematical Computations*, Prentice-Hall, Englewood Cliffs, NJ, 1977.
- [4] G.D. Byrne and A.C. Hindmarsh, "Stiff ODE Solvers: A Review of Current and Coming Attractions", *J. Comput. Phys.*, **70**, pp. 1-62, 1987.
- [5] A.R. Mitchell and D.F. Griffiths, *The Finite Difference Method in Partial Differential Equations*, Chap. 5, John Wiley & Sons, 1980.
- [6] I.S. Gradshteyn and I.M. Ryzhik, *Table of Integrals, Series, and Products*, Corrected and enlarged edition, Academic Press, San Diego, CA, 1980.